A case study for optics: The solid immersion microscope

A. Nickolas Vamivakas,[a] Richard D. Younger,[b] Bennett B. Goldberg, Anna K. Swan, M. Selim Ünlü, and Ernest R. Behringer[c]
Departments of Electrical and Computer Engineering and Physics and the Photonics Center, Boston University, 8 Saint Mary's Street, Boston, Massachusetts 02215

Stephen B. Ippolito
IBM T. J. Watson Research Center, 1101 Kitchawan Road, 11-141, Yorktown Heights, New York 10598

(Received 18 September 2007; accepted 23 March 2008)

Microscopes are natural objects of study in introductory and upper level courses that cover optics because they are used in most science and engineering disciplines. The solid immersion microscope has been developed to study a variety of physical systems with high resolution and we suggest its inclusion in upper level optics courses. We briefly describe the solid immersion microscope in the context of geometrical optics and a desktop demonstration. We use the angular spectrum representation to calculate the focal fields produced by a conventional microscope and a solid immersion microscope. We also suggest a simple model for lens aberration and perform numerically the focal field calculations with and without aberrations to enable users to compare the performance of conventional and solid immersion microscopes. These calculations can help users develop intuition about the sensitivity of microscope performance to real-world manufacturing tolerances and to the limitations and capabilities of microscopy. © *2008 American Association of Physics Teachers.*
[DOI: 10.1119/1.2908186]

I. INTRODUCTION

Upper level optics courses present an excellent opportunity for instructors to teach concepts that are applicable in a wide array of technologies. For example, image formation is the basis of microscopy and satellite surveillance; interference is the basis of thin film spectral filters and sensitive optical fiber gyroscopes; and diffraction is the basis of grating spectroscopy.[1] Within the past decade, new technologies such as Digital Versatile Disc (DVD) optical heads, digital micromirror arrays,[2] and optically interrogated microfluidic cells[3] have been developed by combining microfabrication techniques and optical elements, demonstrating the continuing relevance of optics.

Microscopy is used in cutting edge research and technologies; there are strong connections between microscopy and core areas of physics, including electromagnetism and quantum mechanics; and microscope images convey significant information with great visual impact. For these reasons we suggest that the upper level optics course be made more attractive by providing further coverage of microscopy. Students should also be encouraged to develop a sense of what issues are involved in optical instrument design and should begin to develop intuition about the inherent limitations and sensitivities of optical instruments. A recent paper[4] describes a project for building a confocal microscope.

Current research and development utilizes many different far-field microscopy techniques in scientific and engineering disciplines in the service of nanoscience and nanotechnology. The techniques are as varied as their intended use: for example, wide field, fluorescence, and confocal microscopies.[5] Users of these techniques are often primarily concerned with spatial resolution. For diffraction-limited imaging, the smallest feature that can be resolved has a lateral spatial extent of approximately[6] $\lambda_0/(2\ \mathrm{NA})$, where λ_0 is the free space wavelength of the illumination. The numerical aperture of the imaging system, $\mathrm{NA}=n\sin\alpha$, is characterized by the index of refraction n of the region between the object and the imaging system (that is, the object space) and by the angular semiaperture for light collection α. This expression suggests three ways to decrease the size of the smallest resolvable feature: decrease the wavelength of the illumination, increase the index of refraction of the object space, and increase the angular semiaperture for light collection.

An example of decreasing the illumination wavelength to reduce the size of the smallest resolvable feature is the development of the DVD to succeed the compact disc (CD). DVD players use an illumination wavelength of $\lambda_0=635$ or 650 nm, and CD players use an illumination wavelength of $\lambda_0=780$ nm.[7] Another example of decreasing the illumination wavelength is the development of the scanning electron microscope. Although a conventional light microscope can use illumination with wavelengths as low as $\approx$400 nm, a scanning electron microscope uses electrons with de Broglie wavelengths of less than 0.1 nm, enabling the acquisition of images of higher resolution.[8]

Oil immersion objectives have been designed and constructed to increase the index of refraction of the object space since the 19th century.[9] The oil used with such objectives has an index of refraction that matches that of microscope coverslips to eliminate reflections, and so the index of refraction of the object space is limited to that of the coverslips, that is, $n_{\mathrm{coverslip}}\approx 1.5$. Water immersion objectives were also developed during the 19th century; these are more convenient for use with aqueous biological samples although the smaller index of refraction of water, $n_{\mathrm{water}}\approx 1.33$, produces a smaller improvement of resolution.

In 1990 Mansfield and Kino described a way to increase the index of refraction of the object space using a hemispherical solid immersion lens.[10] This lens images surface objects located at the center of curvature of a solid planoconvex lens [see Fig. 1(b)]. By increasing the index of refraction from $n_{\mathrm{air}}=1$ to the index of refraction of the hemispherical solid immersion lens, n_{SIL}, the smallest feature that can be resolved has a lateral spatial extent of approximately $\lambda_0/(2n_{\mathrm{SIL}}\sin\alpha)$. Hence, the resolution is increased by a fac-

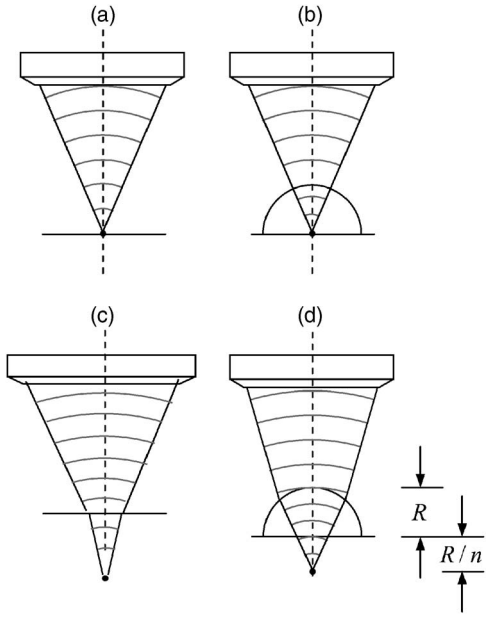

Fig. 1. Ray diagram of light focusing in (a) a conventional microscope, (b) a solid immersion lens microscope, (c) a subsurface microscope, and (d) a numerical aperture increasing lens microscope.

tor of n_{SIL} compared to the case without the hemispherical solid immersion lens. In contrast to the fluid immersion lenses we have described, the resolution increase is limited only by the refractive index of the material used to construct the lens: for example, LaSFN9 glass has $n=1.85$ for visible radiation of free space wavelength $\lambda_0=589$ nm and Si has $n\approx 3.5$ for infrared radiation at $\lambda_0=1800$ nm. The solid immersion lens technique has been demonstrated for CD ROM and magneto-optical disk storage,[11] and has also been used to detect fluorescence from dye-doped 110 nm diameter polystyrene nanospheres[12] and photoluminescence from single quantum dots.[13,14]

A hemispherical solid immersion lens can also be used to image subsurface objects.[15] In a conventional optical microscope focused below a dielectric boundary, as shown in Fig. 1(c), refraction at the boundary reduces the object space numerical aperture according to Snell's law. Incorporation of a hemispherical solid immersion lens with a refractive index n_{SIL} which exactly matches the index of refraction of the substrate $n_{substrate}$ circumvents the reduction in object space numerical aperture by altering the planar boundary geometry. If the optical contact with the substrate is perfect (that is, effectively there is no interface), the resolution is improved by a factor of approximately n_{SIL}. The enhancement is entirely due to the increase in angular semiaperture α; there is no change in the object space refractive index. When used to image subsurface objects, we refer to the hemispherical solid immersion lens as a numerical aperture increasing lens.[16]

Figure 2 presents reflected light images of static random access memory in a Si integrated circuit fabricated with a 0.18 μm process. The device layer of a Si integrated circuit is buried beneath metal layers from above (making optical access impossible) and a Si substrate from below. When imaging the Si device layer through the Si substrate, the device layer is a prototypical subsurface structure. The image in Fig. 2(a) is acquired with a 0.4 numerical aperture 100× microscope objective and no numerical aperture increasing lens,

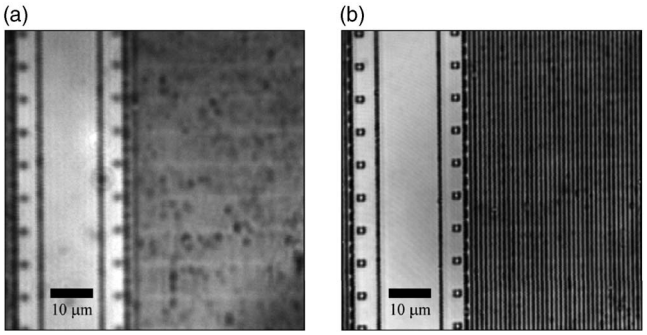

Fig. 2. Images of SRAM in a Si integrated circuit fabricated with a 0.18 μm process taken with (a) a 0.5 numerical aperture 100× microscope objective, (b) a 0.26 numerical aperture 10× microscope objective and a Si numerical aperture increasing lens resulting in a numerical aperture of 3.3.

and the image in Fig. 2(b) is acquired with a 0.26 numerical aperture 10× microscope objective and a Si numerical aperture increasing lens resulting in NA=3.3. The qualitative improvement in the numerical aperture increasing lens image is impressive.

To summarize, solid immersion lenses used with conventional microscopes can be used to obtain images with better resolution than conventional microscopes. In addition, when used as numerical aperture increasing lenses, such lenses not only attain higher resolution but also collect more light from subsurface objects than a conventional microscope. The increases in resolution and light collection are the primary reasons why these lenses have been used in commercial instruments for integrated circuit failure analysis[17] and why we think they deserve attention in upper-level optics courses.

This paper has three major objectives. First, we describe the solid immersion lens microscope in the context of geometrical optics and describe its desktop demonstration. Second, we describe the angular spectrum representation and its implementation. Finally, we illustrate how students can be guided to build intuition about the limitations and sensitivities of solid immersion lens microscopes and other high aperture microscopes by using numerical calculations to model microscope performance. The calculations are intended to complement the excellent WebTOP three-dimensional visualizations developed by Foley *et al.*[18]

The organization of the paper is as follows. Section II gives a brief description of a solid immersion lens microscope and desktop demonstration of such a microscope. Section III describes the angular spectrum representation and its application to a conventional microscope and a solid immersion lens microscope. Section IV presents the results of the numerical calculations, and discusses how the calculations may be used to develop intuition about far-field microscopes in general and microscopes that use solid immersion lenses or numerical aperture increasing lenses in particular. We conclude with a summary in Sec. V.

II. THE SOLID IMMERSION LENS MICROSCOPE

A conventional microscope, as described in both introductory and upper-level undergraduate textbooks,[19,20] consists of two lenses: an eyepiece and an objective. The objective is the more important component, and practicing microscopists select microscope objectives on the basis of magnification, numerical aperture (NA), spectral characteristics, and working

distance (the distance from the end of the objective to the focal plane). For a given magnification, an objective with the highest useable NA that satisfies the requirements for spectral sensitivity and working distance is selected. When using a hemispherical solid immersion lens, a working distance of at least the radius, R, of the solid immersion lens is required. If the lens and the sample with which it shares optomechanical contact are placed into a cryostat to cool the sample (for example, for photoluminescence measurements), the working distance must be significantly larger. This requirement further constrains the choice of microscope objective.

For a hemispherical solid immersion lens in perfect optomechanical contact with a substrate of equal refractive index there are two solutions[16] for point-to-point (that is, stigmatic) imaging assuming the geometrical optics approximation: the first places the object at the center of curvature of the lens, and the second places the object at a depth of R/n_{SIL} below the center of curvature of the lens. The first (second) solution has been referred to as the *central* (*aplanatic*) solution.[16] As described in Sec. I, these solutions are characterized by a lateral resolution that is increased by a factor of n_{SIL} relative to that in the absence of the hemispherical solid immersion lens. The lateral magnification of the central (aplanatic) solution is increased by a factor of n_{SIL} (n_{SIL}^2) compared to the absence of the hemispherical solid immersion lens.

A desktop demonstration of the central solution involves the acquisition of a compact microscope with a reticle and base (Edmund Optics NT61-210) together with a hemispherical BK-7 glass lens (Edmund Optics NT45-937). We can place a piece of graph paper with a grid pattern of 0.1 mm pitch beneath the microscope and bring the pattern into focus by adjusting the vertical position of the microscope tube. We note the number of grid lines that correspond to a portion of the reticle and then place the hemispherical solid immersion lens underneath the microscope. The glass lens has a refractive index of approximately 1.5 and, hence, we expect to observe an image of the grid that is magnified by this factor in comparison to the original image obtained without the solid immersion lens. We can check whether this magnification is achieved by comparing the number of grid lines that fit into the same portion of the reticle. Although somewhat expensive for a single demonstration, it effectively illustrates the solid immersion lens principle and can be passed from student to student during class.[21]

III. THEORY

We present a synthesis of the approaches of Wolf,[22] Richards and Wolf,[23] and Novotny and Hecht[24] to describe the angular spectrum representation in a way that is accessible to upper-level undergraduate students. The angular spectrum representation is a description of an electromagnetic field in terms of a superposition of plane and evanescent waves. From this representation we obtain an expression for the electric field in the far-field limit and use this expression to propagate a beam through a focusing lens and then through either a planar interface or a spherical interface. The propagation through the planar interface models the focusing of light onto a microscope slide, and the propagation through the spherical interface models the focusing of light onto a solid immersion lens. Ultimately, we seek to calculate the focal fields to estimate the resolution of conventional and solid immersion lens microscopes.

A. Angular spectrum representation

We are interested in calculating the electric field $\mathbf{E}$ at a point $P=(x,y,z)$ due to the electric field defined throughout the plane $(x,y,z=0)$ in a material that is assumed to be homogeneous, isotropic, linear, and source-free. We assume that the electric field is monochromatic with angular frequency ω, that is, $\mathbf{e}(x,y,z,t)=\mathbf{E}(x,y,z)e^{-i\omega t}$. Given these assumptions, the time-independent part of the electric field must satisfy the vector Helmholtz equation

$$(\nabla^2 + k^2)\mathbf{E}(x,y,z) = 0, \tag{1}$$

where $k=n_1(2\pi/\lambda_0)=\omega/v$, n_1 is the index of refraction of the material, λ_0 is the free space wavelength of the field, and v is the speed of light in the material. Wolf has shown[25] that when the field propagates toward $z=+\infty$ (and there is no reflected wave traveling toward $z=-\infty$), $\mathbf{E}(x,y,z)$ may be represented by

$$\mathbf{E}(x,y,z) = \int_{-\infty}^{\infty}\int_{-\infty}^{\infty} e^{i(k_x x + k_y y)}\hat{\mathbf{E}}(k_x,k_y;0)e^{ik_z z}dk_x dk_y, \tag{2}$$

where

$$k_z = \begin{cases} [k^2 - (k_x^2 + k_y^2)]^{1/2} & \text{if } k^2 \geq k_x^2 + k_y^2 \\ i[(k_x^2 + k_y^2) - k^2]^{1/2} & \text{if } k^2 < k_x^2 + k_y^2. \end{cases} \tag{3}$$

$\hat{\mathbf{E}}(k_x,k_y;0)$ is called the angular spectrum because it specifies the amplitudes of the constituent waves characterized by different combinations of wavenumbers k_x, k_y, and k_z and, therefore, different wave vectors $\mathbf{k}=(k_x,k_y,k_z)$ and corresponding propagation directions for each vector component of the electric field. Equation (2) is the angular spectrum representation of the field $\mathbf{E}(x,y,z)$. The utility of Eq. (2) is that knowledge of the angular spectrum $\hat{\mathbf{E}}(k_x,k_y;0)$ in one plane $[(x,y,z=0)]$ enables the calculation of $\mathbf{E}$ anywhere in a homogeneous, isotropic, linear, and source-free material.

The angular spectrum representation is not the same as the Fourier transform representation of $\mathbf{E}$ because Eq. (2) does not include an integration over k_z. It is also important to realize that the angular spectrum representation includes contributions from all possible wave vectors $\mathbf{k}$, that is, contributions from both propagating plane waves and decaying evanescent waves. If $k^2 \geq k_x^2+k_y^2$, then k_z is real and $\hat{\mathbf{E}}$ is associated with a homogeneous wave[26] propagating toward $z=+\infty$. If $k^2 < k_x^2+k_y^2$, then k_z is imaginary and $\hat{\mathbf{E}}$ is associated with an inhomogeneous wave[26] decaying toward $z=+\infty$ or growing without bound toward $z=-\infty$.

To proceed we seek an expression for $\hat{\mathbf{E}}(k_x,k_y;0)$. Such an expression can be obtained by using the fact that we are ultimately interested in calculating the electric field at points (x,y,z) that satisfy $k(x^2+y^2+z^2)^{1/2}=kr \gg 1$, where the evanescent components $(k^2 < k_x^2+k_y^2)$ make no contribution. That is, we are interested in calculating the field at a location (for example, the focus of a microscope objective) that is far, on the scale of the wavelength, from the surface where the field is known (for example, the back focal plane of the microscope objective). We denote the electric field at the location where it is known by $\mathbf{E}_\infty$, take the limit $kr \to \infty$, and write Eq. (2) as

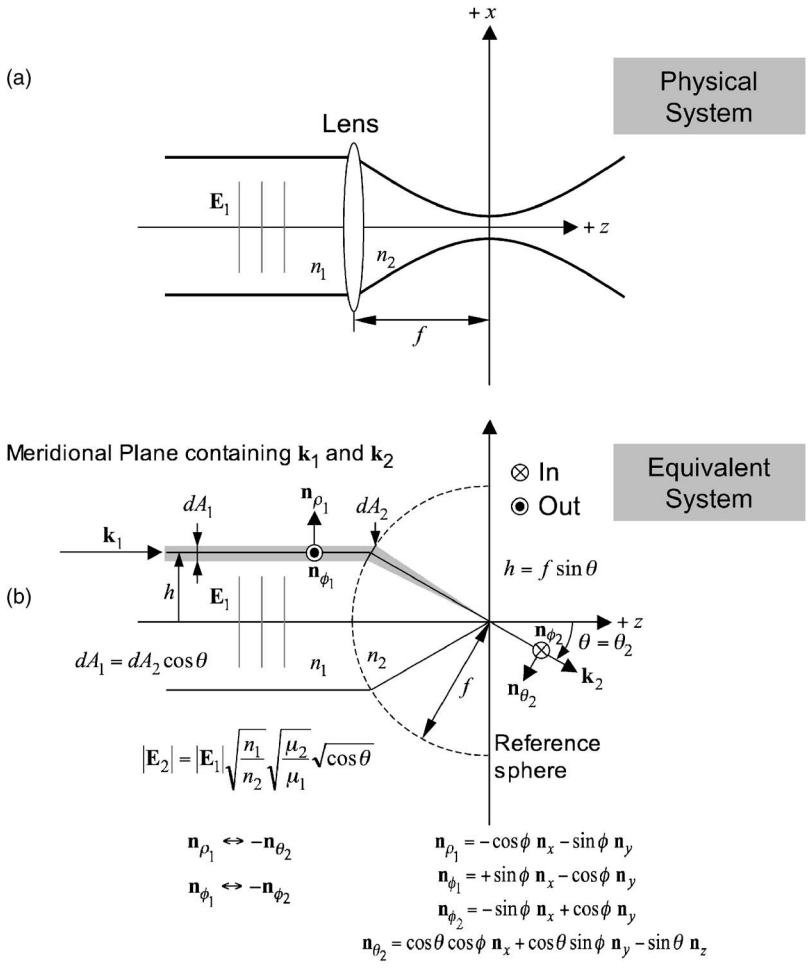

Fig. 3. The system under consideration and its equivalent within the domain of geometrical optics. (a) In the physical system a lens focuses a plane wave to a spot of finite size. (b) In the equivalent system rays corresponding to the incoming plane wave encounter a spherical reference surface and are subsequently focused to a point. The incident and refracted rays are in the meridional plane and obey both the sine condition and intensity law.

$$\mathbf{E}_\infty = \lim_{kr\to\infty} \int\int_{k_x^2+k_y^2\le k^2} e^{i(k_x x+k_y y+k_z z)} \hat{\mathbf{E}}(k_x,k_y;0)\, dk_x dk_y, \quad (4)$$

which, by applying the method of stationary phase,[27] yields the asymptotic approximation

$$\mathbf{E}_\infty(u_x,u_y,u_z) = -2\pi i k u_z \hat{\mathbf{E}}(ku_x,ku_y;0)\frac{e^{ikr}}{r}, \quad (5)$$

where

$$u_x = \frac{x}{r}, \quad u_y = \frac{y}{r}, \quad u_z = \frac{z}{r}. \quad (6)$$

Equation (5) is a significant result. Physically, the field at a point P_∞ in the far zone is given by a weighted, single plane wave with wave vector $\mathbf{k}=k\mathbf{u}=(ku_x,ku_y,ku_z)$ traveling directly toward P_∞, with the weight $-2\pi i k u_z \hat{\mathbf{E}}(ku_x,ku_y;0)/r$ determined in part by the angular spectrum component corresponding to that direction. [An alternative point of view is that the field at point P_∞ is given by a weighted, single spherical wave with weight $-2\pi i k u_z \hat{\mathbf{E}}(ku_x,ku_y;0)$.] This result is obtained because all other plane waves destructively interfere at P_∞. If we relabel $ku_x \to k_x$, $ku_y \to k_y$, and $ku_z \to k_z$ and then substitute Eq. (5) into Eq. (2), we find

$$\mathbf{E}(x,y,z) = \frac{ire^{-ikr}}{2\pi} \int\int_{k_x^2+k_y^2\le k^2} \mathbf{E}_\infty(k_x,k_y) e^{i(k_x x+k_y y+k_z z)} \times \frac{1}{k_z} dk_x dk_y, \quad (7)$$

where we have written $\mathbf{E}_\infty(k_x/k,k_y/k,k_z/k)=\mathbf{E}_\infty(k_x,k_y)$. Note that the arguments of $\mathbf{E}_\infty$ depend only on the direction of the plane wave propagation and not on the magnitude of the wave vector. We have suppressed k_z in $\mathbf{E}_\infty$ because it is a function of k, k_x, and k_y. Equation (7) is the electric field $\mathbf{E}$ at a point (x,y,z) far from the surface at which the angular spectrum is known, and is valid for a monochromatic field propagating toward $z=+\infty$ in a homogeneous, isotropic, linear, source-free material. We will use this expression in the following to calculate the electric field in the focal plane of a lens.

B. Focal fields

Our aim in this section is to describe the propagation of a monochromatic field from one material, through a cylindrically symmetric aplanatic lens of focal length f, and into a second material to obtain an expression for the transmitted

field. We then use Eq. (7) to calculate the field in the second material near the focal point of the lens. As shown in Fig. 3, we assume that the index of refraction of the material in front (back) of the lens is n_1 (n_2). If we assume that geometrical optics is valid (that is, $k \to \infty$), then the action of the lens can be described using the sine condition together with the intensity law (both defined in the next paragraph).[28] In essence, the physical lens is replaced by an equivalent system, also shown in Fig. 3, that obeys the sine condition and the intensity law.

The sine condition requires each ray impinging upon, or exiting from, the focus to intersect its conjugate ray (which propagates parallel to the optical axis) at the surface of a sphere of radius f known as the Gaussian reference sphere. The sine condition is [see Fig. 3(b)]

$$h = f \sin\theta, \tag{8}$$

where h is the distance from the z-axis to the conjugate ray and θ is the angle that the wave vector of the refracted ray, $\mathbf{k}_2$, makes with the $+z$ axis.

The intensity law, as shown in Fig. 3(b) for ray bundles refracting across the Gaussian reference sphere, is an expression of conservation of energy. In the absence of absorption, the rate at which energy carried by a ray bundle passes through a differential area element in one material is equal to the rate at which energy carried by the same ray bundle passes through the corresponding differential area element in a second material. It allows us to relate the magnitude of the electric field associated with the ray in material 1 to that in material 2,

$$|\mathbf{E}_2| = |\mathbf{E}_1| \left(\frac{\mu_1}{\mu_2}\right)^{1/4} \sqrt{\frac{n_1}{n_2}} \sqrt{\cos\theta}, \tag{9}$$

where we have used $n_j = c/v_j = \sqrt{\mu_j \epsilon_j}$, $j = 1, 2$. Because the magnetic permeability at optical frequencies of optical materials such as glass, index-matching fluid, and bulk semiconductors have nearly identical values, the factor $(\mu_2/\mu_1)^{1/4} \approx 1$ and is dropped from the following.

We now express the incident electric field $\mathbf{E}_1$ in terms of the radial and azimuthal (p and s) polarization components in anticipation of a subsequent interaction with an interface,

$$\mathbf{E}_1 = \mathbf{E}_1^{(s)} + \mathbf{E}_1^{(p)} = (\mathbf{E}_1 \cdot \mathbf{n}_{\phi_1})\mathbf{n}_{\phi_1} + (\mathbf{E}_1 \cdot \mathbf{n}_{\rho_1})\mathbf{n}_{\rho_1}, \tag{10}$$

where $\mathbf{n}_{\phi_1}$ and $\mathbf{n}_{\rho_1}$ are the cylindrical coordinate unit vectors referred to the symmetry axis of the lens. The ray described by the field $\mathbf{E}_1$ and wave vector $\mathbf{k}_1$ is shown in Figs. 3(b) and 4.

We now obtain an expression for the vector field after it has traversed the Gaussian reference sphere. Upon encountering the Gaussian reference sphere, the incident ray is refracted and perhaps partially transmitted so that it is now described by the field $\mathbf{E}_2$ and wave vector $\mathbf{k}_2$. The effect of refraction is the mapping of the cylindrical coordinate unit vectors onto the spherical coordinate vectors $\mathbf{n}_{\phi_2}$ and $\mathbf{n}_{\theta_2}$ by $\mathbf{n}_{\phi_1} \to -\mathbf{n}_{\phi_2}$ and $\mathbf{n}_{\rho_1} \to -\mathbf{n}_{\theta_2}$. We use Eqs. (9) and (10), the mapping, and take into account the possibility of partial transmittance of the field to express the transmitted (that is, refracted) electric field $\mathbf{E}_2$ as

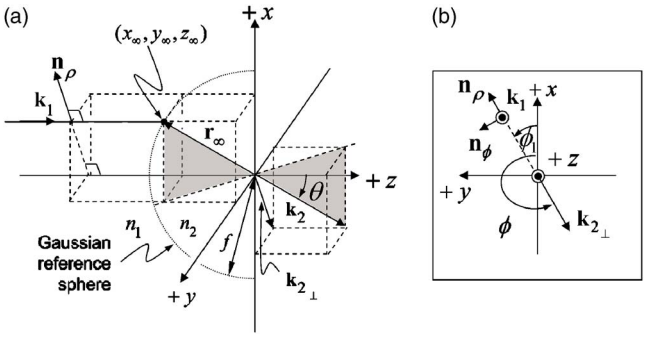

Fig. 4. A perspective of the refraction occurring at the Gaussian reference sphere a radial distance f from the coordinate origin. (a) Incident wave vector $\mathbf{k}_1$ refracts across the reference sphere at a point $\mathbf{r}_\infty$. The refracted wave vector $\mathbf{k}_2$ propagates with spherical angular coordinates (ϕ, θ). (b) Projection of the component of $\mathbf{k}_2$ parallel to the xy-plane, perpendicular to the z-axis. The projection illustrates the relation between the azimuthal coordinate ϕ_1 in region 1 of the optical system to the azimuthal coordinate ϕ defining the propagation direction of wave vector $\mathbf{k}_2$ in region 2 of the optical system.

$$\mathbf{E}_2 = -[t_{12}^{(s)}(\mathbf{E}_1 \cdot \mathbf{n}_{\phi_1})\mathbf{n}_{\phi_2} + t_{12}^{(p)}(\mathbf{E}_1 \cdot \mathbf{n}_{\rho_1})\mathbf{n}_{\theta_2}] \sqrt{\frac{n_1}{n_2}} \sqrt{\cos\theta}, \tag{11}$$

where $t_{12}^{(s)}$ and $t_{12}^{(p)}$ are the transmission coefficients of the lens for the s- and p-polarized field components, respectively.

Because of the transformation of the incident plane wave into a converging spherical wave, it is convenient to express $\mathbf{E}_2$ in terms of spherical angular coordinates. We do so by expressing the unit vectors $\mathbf{n}_{\rho_1}$, $\mathbf{n}_{\phi_1}$, $\mathbf{n}_{\phi_2}$, and $\mathbf{n}_{\theta_2}$ in terms of the spherical coordinates $(\theta_2, \phi_2) = (\theta, \phi)$ describing the direction of $\mathbf{k}_2$, and the Cartesian unit vectors $\mathbf{n}_x$, $\mathbf{n}_y$, and $\mathbf{n}_z$ noting that $\phi_1 = \phi - \pi$ from geometry [see Fig. 4(b)]. Equation (11) yields

$$\mathbf{E}_2 = -\left[[t_{12}^{(s)}\mathbf{E}_1 \cdot \mathbf{n}_{\phi_1}] \begin{pmatrix} -\sin\phi \\ \cos\phi \\ 0 \end{pmatrix} + [t_{12}^{(p)}\mathbf{E}_1 \cdot \mathbf{n}_{\rho_1}] \begin{pmatrix} \cos\phi\cos\theta \\ \sin\phi\cos\theta \\ -\sin\theta \end{pmatrix} \right] \sqrt{\frac{n_1}{n_2}} \sqrt{\cos\theta}. \tag{12}$$

To calculate the focal fields, we substitute Eq. (12) into Eq. (7). Although this calculation does not present any special difficulties, we must reconcile the description of $\mathbf{E}_2$, expressed in terms of the spherical angular coordinates in Eq. (12), with the angular spectrum representation description in which $\mathbf{E}_2$ is expressed in terms of the Cartesian components of $\mathbf{k}_2$. We give an explicit example in the following to show how this reconciliation is achieved so that the focal field can be calculated in practice when we choose the incident field to be a plane wave polarized in the x direction such that

$$\mathbf{E}_1 = E_1(\theta, \phi)\mathbf{n}_x. \tag{13}$$

We replace $\mathbf{E}_\infty$ in Eq. (7) and note that the Cartesian components of $\mathbf{k}_2$, denoted as $k_{2_x} = k_x$, $k_{2_y} = k_y$, and $k_{2_z} = k_z$, are related to the spherical coordinates θ and ϕ by

$$k_x = k\sin\theta\cos\phi, \quad k_y = k\sin\theta\sin\phi, \quad k_z = k\cos\theta. \tag{14}$$

The area element $dk_x dk_y$ can be expressed as

$$dk_x dk_y = \cos\theta(k^2\sin\theta\, d\theta\, d\phi). \tag{15}$$

In this way we obtain

$$\mathbf{E}(\rho,\varphi,z) = \frac{ikfe^{-ikf}}{2\pi}\int_0^{\theta_{\max}} d\theta \int_0^{2\pi} d\phi \left[-t_{12}^{(s)}E_1(\theta,\phi)\sin\phi \right] \begin{pmatrix} -\sin\phi \\ \cos\phi \\ 0 \end{pmatrix} + \left[t_{12}^{(p)}E_1(\theta,\phi)\cos\phi \right] \begin{pmatrix} \cos\phi\cos\theta \\ \sin\phi\cos\theta \\ -\sin\theta \end{pmatrix} \times \sqrt{\frac{n_1}{n_2}}\sqrt{\cos\theta}\, e^{ik\rho\sin\theta[\cos(\phi-\varphi)+ikz\cos\theta]}\sin\theta, \tag{16}$$

where r has been set equal to the lens focal length f, $\theta_{\max}$ is the maximum angular semiaperture by the aplanatic focusing lens, $\rho=(x^2+y^2)^{1/2}$, and $\varphi=\tan^{-1}(y/x)$.

To calculate $\mathbf{E}(\rho,\varphi,z)$, we must specify $E_1(\theta,\phi)$. We now make the additional assumption that the incident plane wave has a Gaussian distribution in the transverse plane such that

$$E_1(\theta,\phi) = E_0 e^{-(x^2+y^2)/w_0^2} = E_0 e^{-f^2\sin^2\theta/w_0^2} = E_0 e^{-\sin^2\theta/(f_0\sin\theta_{\max})^2} = E_0 f_{w_0}(\theta), \tag{17}$$

where w_0 is the half-width of the Gaussian distribution and $f_0 \equiv w_0/(f\sin\theta_{\max})$ defines the filling factor. If the filling factor $f_0 \gg 1$ ($f_0 \ll 1$), then the beam cross section is much larger (smaller) than the useable aperture of the lens, that is, the aperture is overfilled (underfilled). The function $f_{w_0}(\theta)$ is referred to as the *apodization function* and describes the profile of the incident field before it is focused (for example, the objective lens of a microscope). We assume this form for $\mathbf{E}_1$ because it is a typical incident field in a practical confocal microscope. It is possible to choose other forms for $\mathbf{E}_1$ (for example, higher order Gaussian modes), and making such choices is a first step toward focal field engineering, a topic of great current interest.[29]

Given the assumed form for $\mathbf{E}_1$, substitution of Eq. (17) into Eq. (16) yields

$$\mathbf{E}(\rho,\varphi;z) = \frac{ikfE_0e^{-ikf}}{2}\sqrt{\frac{n_1}{n_2}} \begin{pmatrix} I_0 + I_2\cos 2\varphi \\ I_2\sin 2\varphi \\ -2iI_1\cos\varphi \end{pmatrix} \tag{18}$$

as shown in Appendix A. Here I_0, I_1, and I_2 are integrals over θ, defined in Appendix A, which depend on the coordinates ρ and z as well as the transmission coefficients $t_{12}^{(s)}$ and $t_{12}^{(p)}$.

C. Focusing through a planar interface

To calculate the focal fields that result upon transmission through a planar interface, it is useful to initially express the field in terms of the Cartesian components of $\mathbf{k}_2$ instead of the spherical coordinates (θ,ϕ). We start by using Eq. (14) to express $\mathbf{E}_2$, given by Eq. (12), in terms of these components,

$$\mathbf{E}_2 = -\left[t_{12}^{(s)}\mathbf{E}_1\cdot\begin{pmatrix} k_y \\ -k_x \\ 0 \end{pmatrix}\begin{pmatrix} -k_y \\ k_x \\ 0 \end{pmatrix} + t_{12}^{(p)}\mathbf{E}_1\cdot\begin{pmatrix} -k_x \\ -k_y \\ 0 \end{pmatrix}\begin{pmatrix} k_xk_z/k \\ k_yk_z/k \\ -k_\perp^2/k \end{pmatrix}\right]\frac{1}{k_\perp^2}\sqrt{\frac{n_1}{n_2}}\sqrt{\frac{k_z}{k}}, \tag{19}$$

where

$$k_\perp^2 = k_x^2 + k_y^2. \tag{20}$$

When the propagating field encounters a planar interface located at $z=z_0$, it may be transmitted and/or reflected. Upon transmission through the interface, each plane wave constituent of the field characterized by the wave vector $\mathbf{k}=(k_x,k_y,k_z)$ is transformed so that $k_z \to k_{3_z}$ and $k \to k_3$ for the terms inside the brackets $[\cdots]$ in Eq. (19). This transformation does not apply to the factor of k_z/k outside the braces because this factor is due to the application of the intensity law when the incident field traversed the reference sphere, that is, to maintain energy conservation. Consequently, the transmitted field $\mathbf{E}_3$ may be expressed as

$$\mathbf{E}_3 = -e^{i(k_z-k_{3_z})z_0}\left[t_{23}^{(s)}t_{12}^{(s)}\mathbf{E}_1\cdot\begin{pmatrix} k_y \\ -k_x \\ 0 \end{pmatrix}\begin{pmatrix} -k_y \\ k_x \\ 0 \end{pmatrix} + t_{23}^{(p)}t_{12}^{(p)}\mathbf{E}_1\cdot\begin{pmatrix} -k_x \\ -k_y \\ 0 \end{pmatrix}\begin{pmatrix} k_xk_{3_z}/k \\ k_yk_{3_z}/k \\ -k_\perp^2/k_3 \end{pmatrix}\right]\frac{1}{k_\perp^2}\sqrt{\frac{n_1}{n_2}}\sqrt{\frac{k_z}{k}}, \tag{21}$$

where $t_{23}^{(s)}$ ($t_{23}^{(p)}$) is the amplitude transmission coefficient of the s-component (p-component) of the field from material 2 to material 3, and the associated phase factor $e^{i(k_z-k_{3_z})z_0}$ results from the position of the interface at $z=z_0$.

To calculate the transmitted field near the focus, we substitute Eq. (21) into Eq. (7) with the additional change that the factor of $k_z z$ in the argument of the exponential phase factor is changed to $k_{3_z}z$ to account for propagation of the field in material 3 (instead of material 2). As in Sec. III B, we provide an explicit example of how such a calculation is done.

We again assume that the incident field has a Gaussian profile and is directed along the x-axis; that is, $\mathbf{E}_1$ is given by Eq. (13). The substitution of Eq. (13) into Eq. (21), together with the assumption $t_{12}^{(s)}=t_{12}^{(p)}=1$, yields

$$\mathbf{E}_3 = e^{2i(k_{z_2}-k_{z_3})z_0}\left[-t_{23}^{(s)}E_0f_{w_0}(\theta)k_y\begin{pmatrix} -k_y \\ k_x \\ 0 \end{pmatrix} + t_{23}^{(p)}E_0f_{w_0}(\theta)k_x\begin{pmatrix} k_xk_{3_z}/k_3 \\ k_yk_{3_z}/k_3 \\ -k_\perp^2/k_3 \end{pmatrix}\right]\frac{1}{k_\perp^2}\sqrt{\frac{n_1}{n_2}}\sqrt{\frac{k_z}{k}}. \tag{22}$$

As shown in Appendix B, substitution of Eq. (22) into Eq. (7) yields

$$\mathbf{E}(\rho,\varphi;z) = \frac{ikfE_0e^{-ikf}}{2}\sqrt{\frac{n_1}{n_2}} \times \begin{pmatrix} I_{00t^{(s)}} + I_{01t^{(p)}} + (I_{20t^{(s)}} - I_{21t^{(p)}})\cos 2\varphi \\ (I_{20t^{(s)}} - I_{21t^{(p)}})\sin 2\varphi \\ -2iI_{12t^{(p)}}\cos\varphi \end{pmatrix}. \tag{23}$$

Here $I_{nlt^{(\epsilon)}}$ with $n,l=0,1,2$ and $\epsilon=s,p$ are integrals over θ defined in Appendix B which depend on the coordinates ρ and z as well as the transmission coefficients $t_{23}^{(s)}$ and $t_{23}^{(p)}$.

D. Application to solid immersion lens/NAILs

We saw in Sec. III B how to apply the angular spectrum representation to calculate focal fields in a uniform medium; such fields can be produced when using an oil immersion objective. Another technologically important application of the angular spectrum representation is that of the solid immersion microscope. When the planar surface of a hemispherical solid immersion lens is placed at the focus of a conventional microscope, the convergent rays from the objective are all normally incident on the hemispherical surface of the lens. Consequently, only one transmission amplitude is required to describe all of the rays. Furthermore, the hemispherical surface is an equiphase surface for the field and we can, therefore, use the results of Sec. III B to calculate the fields at the planar surface of the solid immersion lens.

We begin with Eq. (7), which is the electric field beyond the lens (that is, the microscope objective) but not yet in the solid immersion lens. The electric field just inside the hemispherical surface of the solid immersion lens differs from that just outside the lens in two ways: the amplitude is diminished, as accounted for by the transmission amplitude coefficient $t_{23}^{\perp}$ for normal incidence from material 2 to material 3, and by the change in wavenumber from $k_2 \rightarrow k_3 = 2\pi n_{\mathrm{SIL}}/\lambda_0$. The electric field may be written as

$$\mathbf{E}(\rho,\varphi;z) = \frac{ikfE_0e^{-ikf}}{2}\sqrt{\frac{n_1}{n_2}}t_{23}^{\perp}\begin{pmatrix} I_0' + I_2'\cos 2\varphi \\ I_2'\sin 2\varphi \\ -2iI_1'\cos\varphi \end{pmatrix}, \tag{24}$$

where I_n' is the same as I_n for $n=1,2,3$ except that k_2 is replaced by k_3.

So far, all that we have presented assumes an ideal system: a perfectly manufactured solid immersion lens that is perfectly aligned with an illumination beam with a Gaussian profile. Even with the greatest care, such a system is unrealizable in practice because there will be slight imperfections in the lens such as asphericity and surface roughness that degrade the performance of the lens. In addition, when using a hemispherical solid immersion lens as a numerical aperture increasing lens to image subsurface objects, an air gap may exist between the planar surface of the solid immersion lens and the substrate. The presence of a sufficiently large gap can degrade the performance of the lens.[16] The multiple reflections at the interfaces that the solid immersion lens shares with its environment may also degrade performance.

Here we model the aberration that describes solid immersion lens asphericity. The aberration enters into the descriptions given previously though an aberration function Φ that appears in the phase of the exponential in the integrand of the integrals I_n, for example $e^{ikz\cos\theta} \rightarrow e^{i(kz\cos\theta+\Phi)}$. Because the aberration function is present in the phase, we expect that any aberration on the order of the wavelength will strongly influence the intensity in the image region.

We model the asphericity of the solid immersion lens as a deviation δ from the ideal solid immersion lens radius R. This radial deviation is

$$\delta = \Delta R\cos\theta, \tag{25}$$

where $\Delta R>0$ is the maximum deviation. This model of the asphericity produces a solid immersion lens that is elongated along the direction of the symmetry axis. The corresponding aberration function Φ is then obtained by calculating the phase difference that results from the presence of the additional lens material,

$$\Phi = (k_3 - k)\delta = (k_3 - k)\Delta R\cos\theta. \tag{26}$$

This model for the asphericity ignores the small change in the amplitude transmission coefficient that results from the change in incident angle relative to the local surface normal.

IV. RESULTS AND DISCUSSION

The theoretical prescriptions presented in Sec. III were implemented by writing programs in MATLAB.[30] These programs can serve as an aid for those who are learning to design microscopes to achieve specific research goals, for example, imaging subsurface objects that emit infrared radiation. Although the programs implement the specific microscope configurations described in Sec. III, they may be adapted to describe microscopes of different configurations. We explore three examples involving different material combinations in the following.

The first example is that of focusing through a lens into a second material. This situation can arise in optical trapping experiments where a particle suspended in water is trapped in the focused field delivered by a water immersion objective, or in biological imaging when using an oil-immersion objective to obtain high resolution. As a reference case, we consider the focusing into air of a x polarized Gaussian beam through a 20× microscope objective with a numerical aperture of 0.4. This example is intended to mimic the optics in a conventional microscope. The corresponding distribution of $|\mathbf{E}|^2/|\mathbf{E}_{\max}|^2$ in the xy-plane (the focal plane of the objective) is shown in Fig. 5(a). Also shown in Fig. 5 is the xy-plane $|\mathbf{E}|^2/|\mathbf{E}_{\max}|^2$ distribution for focusing into oil [Fig. 5(b)] assuming a 100× microscope objective with NA=1.4 and an object space index of refraction of $n_2=1.518$. The final distribution of $|\mathbf{E}|^2/|\mathbf{E}_{\max}|^2$ in the xy-plane, shown in Fig. 5(c), is for focusing into a Si hemispherical solid immersion lens assuming the same 20× microscope objective (numerical aperture of 0.4) and an object space index of refraction of $n_2=3.5$. In Figs. 5(d)–5(f) we plot linecuts of the focal plane $|\mathbf{E}|^2/|\mathbf{E}_{\max}|^2$ distribution along the lines defined by $(x,y=0,z=0)$ and $(x=0,y,z=0)$. The most salient feature of Fig. 5 is the asymmetry in the focal plane distribution when focusing with a high numerical aperture objective into oil [Figs. 5(b) and 5(e)]. If we apply the Houston criterion,[31] which defines the resolution as the full width of the $|\mathbf{E}|^2/|\mathbf{E}_{\max}|^2$ distribution at half the maximum value, to the linecuts in Fig. 5(e), we find a diffraction-limited resolution of 0.50λ along the x-direction and 0.38λ along the y-direction. Though not obvious in Figs. 5(a), 5(d), 5(c), and

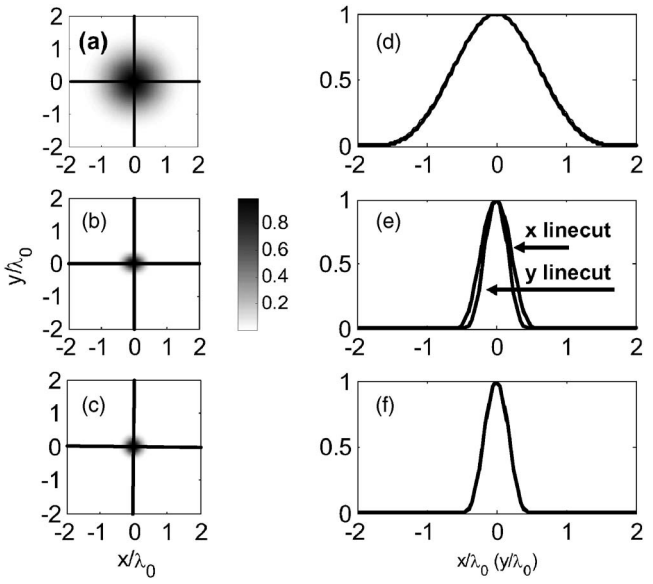

Fig. 5. Plot of $|\mathbf{E}|^2/|\mathbf{E}_{max}|^2$ in the xy-plane for focusing a x-polarized plane wave into (a) air with a 0.4 numerical aperture 20× objective, (c) oil with a 1.4 numerical aperture 100× objective, and (e) Si hemispherical solid immersion lens with a 0.4 numerical aperture 20× objective. The black solid lines in (a), (c), and (e) indicate the directions along which we take linecuts of the $|\mathbf{E}|^2/|\mathbf{E}_{max}|^2$ distribution to generate (b), (d), and (f), respectively. The linecuts are along $(x,y=0,z=0)$ and $(x=0,y,z=0)$.

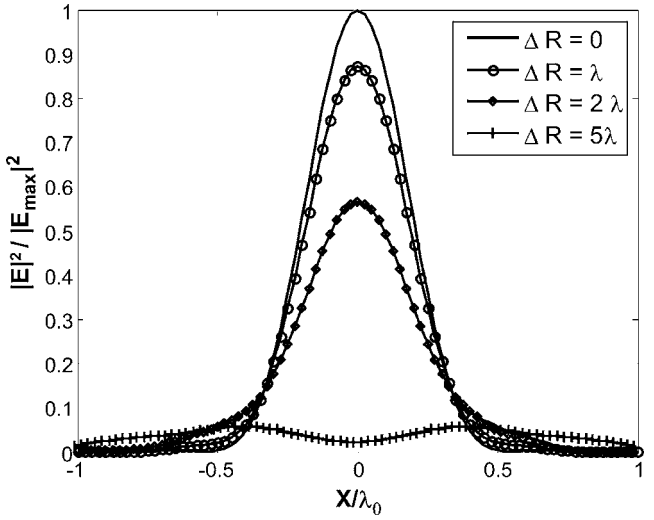

Fig. 7. Linecuts of $|\mathbf{E}|^2/|\mathbf{E}_{max}|^2$ along $(x,y=0,z=0)$ in the xy-plane for focusing into a Si hemispherical solid immersion lens with an aberration of $\Delta R\cos\theta$ for $\Delta R=0,\lambda,2\lambda,5\lambda$.

5(f), there is also a slight asymmetry in the focal plane distributions for the other two cases of focusing with a low numerical aperture objective. In these cases we find in Fig. 5(d) [Fig. 5(f)] a diffraction-limited resolution of $1.44\lambda_0$ $[0.42\lambda_0]$ along the x-direction and $1.40\lambda_0$ $[0.40\lambda_0]$ along the y-direction.

The second example is that of focusing through a planar interface. This situation can arise when focusing through an oil immersion objective and index-matched cover slip into an aqueous sample. Here, we assume a 100× microscope objective with NA=0.92, $n_2=1.517$, and $n_3=1.33$. The resulting intensity distribution of $|\mathbf{E}|^2/|\mathbf{E}_{max}|^2$ in the xy-plane is shown in Fig. 6(a). From the linecuts in Fig. 6(b) we find a diffraction limited resolution of $0.58\lambda_0$ in the x-direction and $0.33\lambda_0$ in the y-direction. In comparison to the case of focusing into oil only we find that the resolution in the x-direction becomes worse, whereas the resolution in the y-direction improves.

The third example is focusing into a Si hemispherical solid immersion lens which deviates from the ideal spherical shape by a smooth radial deviation $\delta=\Delta R\cos\theta$. Because we found nearly symmetric $|\mathbf{E}|^2/|\mathbf{E}_{max}|^2$ distributions in the focal plane for the different values of ΔR, we plot linecuts along $(x,y=0,z=0)$ in Fig. 7 for $\Delta R=0,\lambda_0,2\lambda_0,5\lambda_0$ with all linecuts normalized to the maximum of $\Delta R=0$. As the asphericity increases, the resolution degrades and the field amplitude at the Gaussian focus decreases. When $\Delta R=5\lambda_0$, the aberration has resulted not only in an enlarged focal spot, but also a redistribution of the electromagnetic energy into two side lobes.

These results model the performance of different microscopes as well as the changes in performance when an aberration is introduced and provide an introduction to advanced microscopy concepts for students in the upper level optics courses. Students can use and adapt the MATLAB code to explore situations of their own choosing. It is hoped that

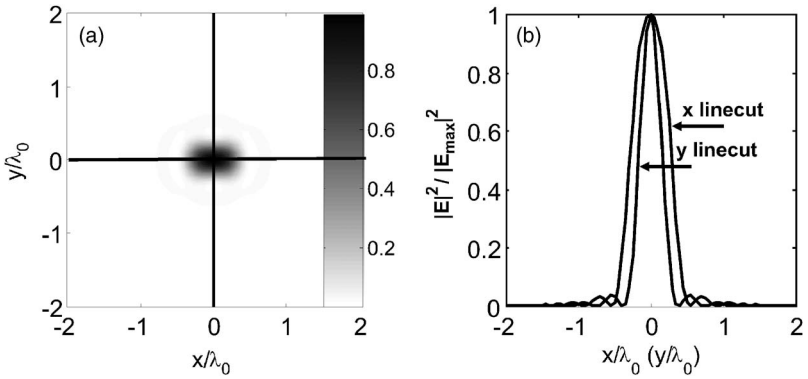

Fig. 6. (a) Plot of $|\mathbf{E}|^2/|\mathbf{E}_{max}|^2$ in the xy-plane for focusing a x-polarized plane wave through oil and a planar interface into water with a 0.92 numerical aperture 100× objective. (b) Linecuts of the $|\mathbf{E}|^2/|\mathbf{E}_{max}|^2$ distribution along the black solid lines in (a). These lines are along $(x,y=0,z=0)$ and $(x=0,y,z=0)$.

such an exploration will inspire students to push the limits of microscopy, and the use of focal fields, perhaps through focal field engineering techniques as in 4π[29,32] or I^5M microscopy[33] and/or making use of nonlinear effects that are the basis of current efforts to beat the diffraction limit.

V. SUMMARY

We have described the solid immersion lens microscope and the angular spectrum representation that is appropriate in upper level undergraduate optics courses, and have illustrated how students might be guided to build their intuition about the limitations and sensitivities of solid immersion lens microscopes by using numerical calculations to model its performance. The calculations show that the solid immersion lens improves the resolution that can be achieved by a conventional microscope although this improvement is sensitive to the dimensions of the solid immersion lens.

It is important for students to have the sense that they are learning concepts that are not only fundamental but are of current interest. Microscopy concepts fit both of these criteria because of the connections to the foundations of physics, and because of the widespread use of microscopes. The topic of microscopy can be presented at varying levels of rigor and is in the reach of upper level undergraduate students. It is empowering for students to realize that they can understand seminal research literature such as the paper by Wolf.[22]

ACKNOWLEDGMENTS

The Boston University portion of this work was supported by the Air Force Office of Scientific Research under Grant No. MURI F-49620-03-1-0379 and by the NSF under Grant No. NIRT ECS-0210752. The Lincoln Laboratory portion of this work was sponsored by the United States Air Force under program FA8721-05-C-0002. The opinions, interpretations, conclusions and recommendations are those of the authors and are not necessarily endorsed by the United States Government. The authors thank Lukas Novotny and Bert Hecht for providing pre-publication drafts of their book. E.R.B. thanks his Boston University colleagues for providing an engaging and stimulating environment during the professional leave granted by Eastern Michigan University. S.B.I. performed the research while at Boston University.

APPENDIX A: MATHEMATICAL DETAILS OF FOCUSED FIELDS

We provide details of how to obtain Eq. (18) from Eq. (16). We begin by substituting Eq. (17) into Eq. (16) and taking terms that depend only on θ out of the integral over ϕ to obtain

$$\mathbf{E}(\rho,\varphi;z) = \frac{ikfE_0e^{-ikf}}{2\pi}\sqrt{\frac{n_1}{n_2}}\int_0^{\theta_{\max}} d\theta f_{w_0}(\theta)\sqrt{\cos\theta}\sin\theta e^{ikz\cos\theta} \times \int_0^{2\pi}\left[-t_{12}^{(s)}\begin{pmatrix}-\sin^2\phi\\ \sin\phi\cos\phi\\ 0\end{pmatrix} + t_{12}^{(p)}\begin{pmatrix}\cos^2\phi\cos\theta\\ \sin\phi\cos\phi\cos\theta\\ -\cos\phi\sin\theta\end{pmatrix}\right] e^{ik\rho\sin\theta\cos(\phi-\varphi)}d\phi. \tag{A1}$$

The integrals over ϕ in Eq. (A1) can be evaluated by using the identities

$$\int_0^{2\pi}\cos n\phi e^{iu\cos(\phi-\varphi)}d\phi = 2\pi(i^n)J_n(u)\cos n\varphi, \tag{A2}$$

$$\int_0^{2\pi}\sin n\phi e^{iu\cos(\phi-\varphi)}d\phi = 2\pi(i^n)J_n(u)\sin n\varphi, \tag{A3}$$

where $J_n(u)$ is the Bessel function of order n, together with the trigonometric identities $\sin^2\phi=(1-\cos 2\phi)/2$, $\sin\phi\cos\phi=(\sin 2\phi)/2$, and $\cos^2\phi=(1+\cos 2\phi)/2$.

If we define the integrals

$$I_0 \equiv \int_0^{\theta_{\max}} d\theta f_{w_0}(\theta)\sqrt{\cos\theta}\sin\theta J_0(k\rho\sin\theta)e^{ikz\cos\theta} \times (t_{12}^{(s)} + t_{12}^{(p)}\cos\theta), \tag{A4}$$

$$I_1 \equiv \int_0^{\theta_{\max}} d\theta f_{w_0}(\theta)\sqrt{\cos\theta}\sin\theta J_1(k\rho\sin\theta)e^{ikz\cos\theta} \times (t_{12}^{(p)}\sin\theta), \tag{A5}$$

$$I_2 \equiv \int_0^{\theta_{\max}} d\theta f_{w_0}(\theta)\sqrt{\cos\theta}\sin\theta J_2(k\rho\sin\theta)e^{ikz\cos\theta} \times (t_{12}^{(s)} - t_{12}^{(p)}\cos\theta), \tag{A6}$$

we can write

$$\mathbf{E}(\rho,\varphi;z) = \frac{ikfE_0e^{-ikf}}{2}\sqrt{\frac{n_1}{n_2}}\begin{pmatrix}I_0 + I_2\cos 2\varphi\\ I_2\sin 2\varphi\\ -2iI_1\cos\varphi\end{pmatrix}. \tag{A7}$$

APPENDIX B: TRANSMISSION THROUGH A PLANAR INTERFACE

Here we provide details of how to obtain Eq. (23) from Eq. (22). We begin by expressing Eq. (22) in terms of the spherical angular coordinates (θ,ϕ). To do so, we make use of Eq. (14) and the relation

$$\cos\theta_3 = (1-\sin^2\theta_3)^{1/2} = \left(1-\frac{n_2^2\sin^2\theta}{n_3^2}\right)^{1/2} = \frac{n_2}{n_3}\left(\frac{n_3^2}{n_2^2}-\sin^2\theta\right)^{1/2} = \frac{n_2}{n_3}g(\theta) \tag{B1}$$

to obtain

$$\mathbf{E}_3 = e^{ik[\cos\theta - g(\theta)]z_0} E_0 f_{w_0}(\theta) \left[t_{23}^{(s)} \begin{pmatrix} \sin^2\phi \\ -\cos\phi\sin\phi \\ 0 \end{pmatrix} + t_{23}^{(p)} \begin{pmatrix} \cos^2\phi (n_2/n_3) g(\theta) \\ \cos\phi\sin\phi (n_2/n_3) g(\theta) \\ -\cos\phi\sin\theta (n_2/n_3) \end{pmatrix} \right] \sqrt{\frac{n_1}{n_2}} \sqrt{\cos\theta}. \quad \text{(B2)}$$

If we use several trigonometric identities as in Appendix A, we can write Eq. (B2) as

$$\mathbf{E}_3 = e^{ik[\cos\theta - g(\theta)]z_0} \frac{E_0}{2} f_{w_0}(\theta) \left[t_{23}^{(s)} \begin{pmatrix} (1-\cos 2\phi) \\ -\sin 2\phi \\ 0 \end{pmatrix} + t_{23}^{(p)} (n_2/n_3) \begin{pmatrix} (1+\cos 2\phi) g(\theta) \\ \sin 2\phi g(\theta) \\ -2\cos\phi\sin\theta \end{pmatrix} \right] \sqrt{\frac{n_1}{n_2}}, \sqrt{\cos\theta}. \quad \text{(B3)}$$

The transmitted field $\mathbf{E}_t$ can be calculated by adapting Eq. (7) as described in Sec. III C,

$$\mathbf{E}_t(x,y,z) = \frac{ife^{-ikf}}{2\pi} \int\int_{k_x^2+k_y^2 \le k^2} \mathbf{E}_3(k_x,k_y) e^{i(k_x x + k_y y + k_{3_z} z)} \times \frac{1}{k_z} dk_x dk_y. \quad \text{(B4)}$$

We express $\mathbf{E}_t$ in terms of cylindrical coordinates, write the integral in terms of spherical coordinates, evaluate the integrals over ϕ via Eqs. (A2) and (A3), and define the following integrals:

$$I_{n0t^{(\epsilon)}} \equiv \int_0^{\theta_{\max}} d\theta f_{w_0}(\theta) \sqrt{\cos\theta} \sin\theta e^{ik\cos\theta z_0} e^{ikg(\theta)(z-z_0)} \times J_n(u) t_{23}^{(\epsilon)} \sin\theta, \quad \text{(B5)}$$

$$I_{n1t^{(\epsilon)}} \equiv \int_0^{\theta_{\max}} d\theta f_{w_0}(\theta) \sqrt{\cos\theta} \sin\theta e^{ik\cos\theta z_0} e^{ikg(\theta)(z-z_0)} \times J_n(u) t_{23}^{(\epsilon)} (n_2/n_3) g(\theta), \quad \text{(B6)}$$

$$I_{n2t^{(\epsilon)}} \equiv \int_0^{\theta_{\max}} d\theta f_{w_0}(\theta) \sqrt{\cos\theta} \sin\theta e^{ik\cos\theta z_0} e^{ikg(\theta)(z-z_0)} \times J_n(u) t_{23}^{(\epsilon)} (n_2/n_3) \sin\theta, \quad \text{(B7)}$$

where $n=0,1,2$, $\epsilon=s,p$, and $u \equiv k\rho\sin\theta$. We finally obtain Eq. (23):

$$\mathbf{E}(\rho,\varphi;z) = \frac{ikfE_0 e^{-ikf}}{2} \sqrt{\frac{n_1}{n_2}} \times \begin{pmatrix} I_{00t^{(s)}} + I_{01t^{(p)}} + (I_{20t^{(s)}} - I_{21t^{(p)}})\cos 2\varphi \\ (I_{20t^{(s)}} - I_{21t^{(p)}})\sin 2\varphi \\ -2iI_{12t^{(p)}}\cos\varphi. \end{pmatrix}. \quad \text{(B8)}$$

[a] Present address: Cavendish Laboratory, University of Cambridge, JJ Thomson Ave, Cambridge CB3 0HE, UK.
[b] Present address: Lincoln Laboratory, Massachusetts Institute of Technology, Lexington, Massachusetts 02420.
[c] Electronic mail: ebehringe@emich.edu. Present address: Department of Physics and Astronomy, Eastern Michigan University, Ypsilanti, Michigan 48197.

[1] M. Born and E. Wolf, *Principles of Optics* (Cambridge U.P., Cambridge, 2002), 7th expanded ed., Chaps. 6–8.
[2] Texas Instruments, "Single-panel DLP projection system optics," Application Report: Discovery DLPA002 (2005).
[3] G. L. Liu, J. Kim, Y. Lu, and L. P. Lee, "Optofluidic control using photothermal nanoparticles," Nat. Mater. **5**, 27–32 (2006).
[4] P. Xi *et al.*, "The design and construction of a cost-efficient confocal laser scanning microscope," Am. J. Phys. **75**(3), 203–207 (2007).
[5] The websites ⟨www.microscopyu.com⟩ and ⟨www.olympusmicro.com⟩ are valuable resources for learning about microscopy techniques and terms relevant to microscopy in general.
[6] J. Higbie, "Microscope resolution," Am. J. Phys. **49**(1), 40–42 (1981).
[7] The decrease in illumination wavelength is only partially responsible for the large increase in data storage capacity of the DVD compared to the CD. A DVD player also uses a lens with a NA that is a factor of $\frac{4}{3}$ greater than that used by a CD player.
[8] Scanning electron microscopes use electrons with kinetic energies from several hundred eV to tens of keV. The de Broglie wavelength $\lambda = h/p$ of an electron with kinetic energy 500 eV is approximately 0.055 nm. This length is much smaller than the size of the smallest resolvable feature, which in practice is limited by the very low NA of the electron lenses.
[9] See, for example, ⟨micro.magnet.fsu.edu/optics/timeline⟩.
[10] S. M. Mansfield and G. S. Kino, "Solid immersion microscope," Appl. Phys. Lett. **57**(24), 2615–2616 (1990).
[11] Isao Ichimura, Shinichi Hayashi, and G. S. Kino, "High-density optical recording using a solid immersion lens," Appl. Opt. **36**(19), 4339–4348 (1997).
[12] Masahiro Yoshita, Kazuko Koyama, Yuhei Hayamizu, Motoyoshi Baba, and Hidefumi Akiyama, "Improved high collection efficiency in fluorescence microscopy with a Weierstrass-sphere solid immersion lens," Jpn. J. Appl. Phys. **41**(7B), L8580–L860 (2002).
[13] S. Moehl, Hui Zhao, B. Dal Don, S. Wachter, and H. Kalt, "Solid immersion lens-enhanced nano-photoluminescence: Principle and applications," J. Appl. Phys. **93**(10), 6265–6272 (2003).
[14] Z. Liu, B. B. Goldberg, S. B. Ippolito, A. N. Vamivakas, M. S. Ünlü, and R. P. Mirin, "High resolution, high collection efficiency in numerical aperture increasing lens microscopy of individual quantum dots," Appl. Phys. Lett. **87**, 071905-1–3 (2005).
[15] S. B. Ippolito, S. A. Thorne, M. G. Eraslan, B. B. Goldberg, M. S. Ünlü, and Y. Leblebici, "High spatial resolution subsurface thermal emission microscopy," Appl. Phys. Lett. **84**, 4529–4531 (2004).
[16] S. B. Ippolito, B. B. Goldberg, and M. S. Ünlü, "Theoretical analysis of numerical aperture increasing lens microscopy," J. Appl. Phys. **97**, 053105-1–12 (2005).
[17] Hamamatsu μAMOS-200 IC Failure Analysis System.
[18] ⟨http://www.webtop.org⟩.
[19] R. Serway and J. Jewett, *Physics for Scientists and Engineers* (Brooks Cole, New York, 2004), 6th ed., Sec. 36.9.
[20] E. Hecht, *Optics* (Addison-Wesley, San Francisco, 2002), 4th ed., Sec. 5.9.
[21] For an inexpensive demonstration, it may be possible to use hemispherical molds and concentrated gelatin to produce gelatin hemispherical solid immersion lens. See, for example, M. Branca and I. Soletta, "Construction of optical elements with gelatin," Phys. Teach. **41**, 249 (2003).
[22] E. Wolf, "Electromagnetic diffraction in optical systems. I. An integral representation of the image field," Proc. R. Soc. London, Ser. A **253**(1274), 349–357 (1959).
[23] B. Richards and E. Wolf, "Electromagnetic diffraction in optical systems. II. Structure of the image field in an aplanatic system," Proc. R. Soc. London, Ser. A **253**(1274), 358–379 (1959).
[24] L. Novotny and B. Hecht, *Principles of Nano-Optics* (Cambridge U.P., Cambridge, 2006).
[25] E. Wolf, "A scalar representation of electromagnetic fields: II," Proc. Phys. Soc. London **74**, 269–280 (1959).
[26] A homogeneous wave has coincident equiphase and equiamplitude surfaces. An inhomogeneous wave has equiphase surfaces that are different than the equiamplitude surfaces. See Ref. 1, Sec. 1.3.3.

[27] L. Mandel and E. Wolf, *Optical Coherence and Quantum Optics* (Cambridge U.P., New York, 1995), Sec. 3.3.4
[28] Reference 1, Chaps. 4.5.1 and 3.1.2.
[29] C. J. R. Sheppard, G. Calvert, and M. Wheatland, "Focal distribution for superresolving Toraldo filters," J. Opt. Soc. Am. A **15**, 849–856 (1998).
[30] See EPAPS Document No. E-AJPIAS-76-015806 to obtain the Matlab programs used to generate the focal field distributions. For more information on EPAPS, see http://www.aip.org/pubservs/epaps.html.
[31] A. J. den Dekker and A. van den Bos, "Resolution: A survey," J. Opt. Soc. Am. A **14**, 547–557 (1997).
[32] S. W. Hell and J. Wichmann, "Breaking the diffraction resolution limit by stimulated emission," Opt. Lett. **19**, 780–782 (1994).
[33] J. Bewersdorf, R. Schmidt, and S. W. Hell, "Comparison of I^5M and 4Pi-microscopy," J. Microsc. **222**, 105–117 (2006).

Singing Tubes. This is my favorite apparatus for demonstrating beats. The two glass tubes have electrically-heated wire filaments about one quarter of the way up. As the heated air rises, cooler air is drawn up into the bottom, resulting in the formation of eddies in the air, and standing waves in the tubes. The shorter of the tubes has a sliding paper sleeve placed on its upper end. I start with the sleeve all the way down so that the frequency is somewhat higher than that produced by the other tube, and beats are produced. As the sleeve is slid up the tube, the frequency goes down, and eventually the zero beat condition is obtained. Sliding it still further up produces beats once more. The apparatus was in the Central Scientific Company catalogue for many years. In 1940 it cost $31.00. (Photograph and Notes by Thomas B. Greenslade, Jr., Kenyon College)